

Electrolysis for Valorization of Industrially-Sourced Crude Glycerol

Published as part of ACS Sustainable Chemistry & Engineering *special issue* "Advancing a Circular Economy".

Rachel N. Gaines, Adam P. Sibal, Abiela M. Bradley, James J. Griebler, Vijay M. Shah, Bridget E. Friel, Simon A. Rogers, Ashlynn S. Stillwell, and Paul J. A. Kenis*



Cite This: <https://doi.org/10.1021/acssuschemeng.5c03028>



Read Online

ACCESS |

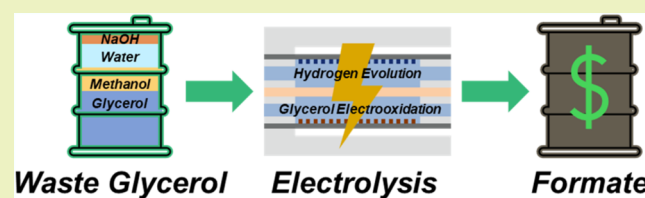
Metrics & More

Article Recommendations

Supporting Information

ABSTRACT: Valorization of waste (crude) glycerol could enhance sustainability of chemical manufacturing and the economics of biodiesel production. Crude glycerol is of low value, and is typically a mixture of glycerol, methanol, water, sodium hydroxide, and residual impurities. This study disentangles the influences of methanol and triglyceride impurities on the electrolytic oxidation of industrially sourced waste glycerol. Data from industrial biodiesel producers uncovered two predominant waste glycerol formulations: methanol-rich and methanol-lean. Electrolysis using synthetic equivalents of these formulations over a nickel catalyst in a flow electrolyzer revealed that performance losses of up to 90% can be avoided in the presence of ≥ 0.5 M methanol. At lower concentrations of methanol, use of a dynamic reactor operation protocol mitigated performance losses. The combination of these results enabled stable multihour electrolytic production of the valuable chemical formate from industrially sourced waste glycerol. These findings provide guidance toward feasible operating conditions and process parameters for the further development of crude glycerol electrolysis in industrial practice.

KEYWORDS: catalysis, biodiesel production, sustainable manufacturing, reaction engineering, process optimization



INTRODUCTION

The production of biodiesel from renewable sources such as soybean oil, tallow, waste cooking oil, and other feedstocks generates approximately 10% byproducts by weight, primarily in the form of a glycerol-rich waste stream. Because biodiesel production is not yet financially competitive with fossil fuel-derived diesel without governmental incentives,^{1–3} converting the low-value waste (i.e., crude) glycerol generated during the production process into value-added products has been proposed to generate additional revenue and bring biodiesel closer to economic viability. Several catalytic approaches have been investigated for the valorization of glycerol to numerous products, and comparisons between these methods is the subject of several reviews.^{4–7} Here, we focus on electro-oxidative (anodic) conversion of glycerol to value-added products, as it can be paired with concurrent value-added cathodic reactions and driven by renewable energy.

Industrially sourced waste glycerol (ISG) from biodiesel production, while variable in its composition, is typically composed of glycerol, methanol, water, and residual base. We found that waste glycerol streams can be categorized into two subtypes: methanol-rich and methanol-lean (vide infra). Methanol-rich waste glycerol is typically produced by low-production-capacity facilities where purification is not cost-effective, whereas methanol-lean waste glycerol is typically produced by intermediate- and high-capacity facilities where additional purification costs for methanol removal can be

justified.⁸ Based on our primary data collection, few U.S. biodiesel facilities purify glycerol streams to 85% purity or higher.

In contrast, the composition of "glycerol" used in most glycerol electrooxidation studies is idealized. Often, they focus on optimization of electrooxidation conditions for >99% pure, neutralized streams, where water and electrolyte (typically base) are added. These efforts neglect the presence of methanol, as well as the alkalinity of the preexisting feed and the level of dilution. Implementing this kind of electrolysis process at scale, which would involve successive energy-intensive water and electrolyte removal and addition steps, would dramatically increase process costs.

Of the few studies that have specifically investigated the direct electrooxidation of low-purity waste glycerol, most evaluate a variety of modified and unmodified platinum-group metal (PGM) catalysts (e.g., Pt, Ir, Au) to understand their performance under oxidative conditions, both in bulk electrolysis and in fuel cells.^{9–21} These catalysts exhibit

Received: April 2, 2025

Revised: August 4, 2025

Accepted: August 5, 2025

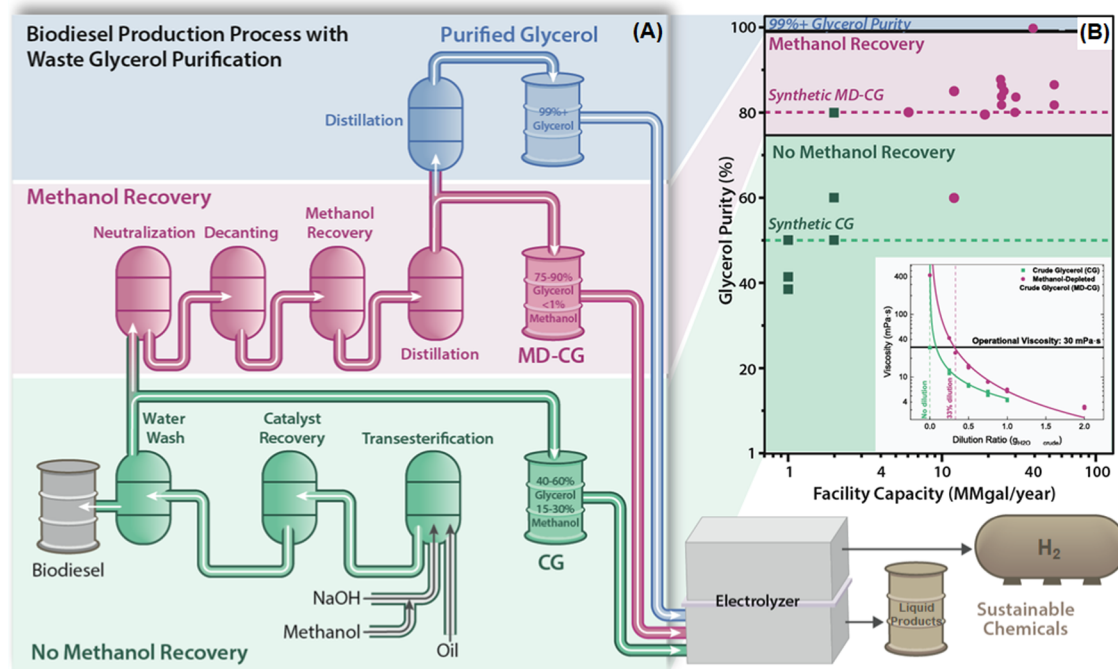


Figure 1. (A) Schematic representation of the biodiesel production process, coupled to waste glycerol purification and subsequent electrocatalytic chemical production. Most literature focuses on purified >99% glycerol, whereas more common waste glycerol compositions are obtained directly after the first water-wash step (crude glycerol, CG; green) or after additional methanol recovery (methanol-depleted crude glycerol, MD-CG; pink). (B) Waste glycerol purity versus facility capacity for 19 surveyed facilities. Most low-volume facilities do not recover methanol from their waste glycerol; most intermediate- and high-volume facilities do. Inset: Viscosity versus dilution ratio for two representative compositions of waste glycerol (crude glycerol, CG; methanol-depleted crude glycerol, MD-CG). Operational viscosity represents the most viscous substance flowable in the flow electrolyzer at a flow rate of 0.5 mL/min. CG is flowable without dilution, whereas MD-CG requires a minimum of 0.33 g water added for every 1 g of waste glycerol to be flowable.

relatively low electrooxidation currents or have limited operational windows in the presence of waste glycerol. Overoxidation and carbon monoxide poisoning are likely the major competing deactivation mechanisms in these experiments; PGM catalysts are well-known to be susceptible to both.²²

Studies that investigate PGM-free catalysts (e.g., stainless steel, Ni) for electrooxidative valorization of waste glycerol first remove methanol from waste glycerol, using evaporation and similar procedures, before performing electrolysis experiments.^{21,23–25} These separation processes add energy consumption and associated costs, limiting scalability of the electrolysis process.

Notably, Velázquez-Hernández, Arjona, and co-workers investigated waste glycerol electrooxidation on modified palladium electrodes using synthetic mixtures of glycerol, methanol, and potassium hydroxide.²⁴ However, the waste glycerol mixtures used contained at least 85% glycerol, reducing the generalizability of their approach *vis à vis* the wide range of industrially sourced waste glycerol compositions (*vide infra*).

To assess the viability of electrooxidative waste glycerol conversion, a systematic investigation of feed compositions representative of waste streams from industrial facilities is necessary. Furthermore, investigation of PGM-free catalysts is critical, both for economic viability and to avoid the negative impacts of overoxidation and carbon monoxide poisoning. Drawing inspiration from prior work,^{26,27} we utilize a nickel catalyst studied extensively for both methanol and glycerol electrooxidation. This prior work included detailed mecha-

nistic pathways for electrooxidation of methanol and glycerol on nickel. Utilizing a nickel catalyst has three key benefits: (1) electrooxidation of both methanol- and glycerol in alkaline conditions on nickel produce the value-added product formate almost exclusively, and any less-oxidized products can be recycled in the same reactor to produce additional formate,^{28–31} reducing separation costs; (2) nickel is robust against both overoxidation and carbon monoxide poisoning, a critical property for stability and thus long-term operation;^{32,33} and (3) nickel is a low-cost, readily available metal compared to other common (including PGM) catalysts, further improving economic viability. Although other products from glycerol electrooxidation have been suggested to be more valuable,^{34–39} the separations cost associated with isolating multiple resultant products of the simultaneous electrooxidation of methanol and glycerol likely outweighs the reportedly higher prices for C₂ and C₃ fine chemicals.⁴⁰ Recently, Kim et al. sought to investigate waste glycerol electrooxidation on nickel in a bicarbonate electrolyte, reportedly to pursue coelectrolysis of CO₂, using a single ‘synthetic crude glycerol’ feed containing glycerol, methanol, potassium hydroxide, and oleate. In most cases, starting from ~10 mA/cm² current densities, they observed a 25–75% loss of activity, which they attributed to deactivation of the nickel catalyst surface.⁴¹ It is likely that the large pH gradient, which can result in, e.g., uneven membrane wetting, catalyst and membrane fouling, and asymmetric ion transfer, lead to some of the reported decay in activity. In lieu of a bicarbonate-based cathodic reaction, the alkaline hydrogen evolution reaction can be used. In doing so, the results of waste glycerol electrolysis

can be clearly deconvoluted from the complexities introduced by these nonuniform operating conditions, and the coproduction of two value-added chemicals (formate and hydrogen) can be performed with higher energy efficiency and less degradation. This reduction in cost, combined with the cost reductions realized by using a waste stream to produce hydrogen,^{42–45} improves the industrial value of the coproduction of hydrogen and formate by waste glycerol electrolysis.

In this work, we demonstrate the stable electrooxidation of waste glycerol available from several U.S. biodiesel manufacturers. We first perform a systematic electrooxidation study of synthetic waste glycerol compositions as are produced by biodiesel manufacturing plants, identifying key operating parameters that address barriers to long-term operation, including poor flowability and activity loss as a function of feed composition. These results lead to insights with respect to the factors that help to retain catalyst activity and product speciation over time. We then leverage this knowledge in the electrooxidation of industrially sourced waste glycerol to the value-added chemical formate, disentangling the influences of impurities and demonstrating stable activity for multiple hours.

RESULTS AND DISCUSSION

Our evaluation of the landscape of industrial waste glycerol compositions, sourced from literature and our primary data collection from industry, reveals the predominance of two compositions: a less purified composition rich in methanol, and a more purified composition lean in methanol. By studying the electrooxidation of synthetic methanol-rich and methanol-lean waste glycerol streams, we identify operating conditions that enable stable electrolysis processes with both feed types for multiple hours. We then leverage these insights to pursue the electrooxidation of industrially sourced waste glycerol.

Assessment of Industrial Waste Glycerol Production. Biodiesel production processes consist of a variety of successive unit operations, in which glycerol byproduct streams are refined to different purities, depending on the size of the producer (Figure 1a). Waste glycerol is collected at different stages, such as after a water wash column (green), after neutralization and methanol recovery via distillation (pink), or after two additional distillation steps (blue). Thus, the composition of industrially sourced waste glycerol can vary dramatically.

To better understand the landscape of glycerol compositions, we requested glycerol composition data from U.S. biodiesel production facilities and combined those primary data with data reported in literature (Figure 1b, Supporting Text S1 and Table S1).^{46,47} Note that only one high-capacity facility out of the 19 included in our analysis purified a portion of their glycerol to ≥99% purity (Figure 1b, blue), indicating the critical need to investigate other waste glycerol compositions. Our data show a clear stratification between the glycerol compositions sourced from low-capacity (≤ 4 million gallons biodiesel produced/year) and high-capacity (> 4 million gallons biodiesel produced/year) biodiesel production facilities.

Low-capacity facilities often lack the resources to invest in additional unit operations for recovery of methanol from their waste glycerol (Figure 1, green). This methanol-rich waste glycerol typically contains 40–60% glycerol and 15–30% methanol. Most of these facilities sell this low-purity glycerol at ~\$0.03/kg. Henceforth, we refer to this *methanol-rich waste*

glycerol, with no methanol recovery beyond the water wash column, as “*crude glycerol*” (CG).

In contrast, high-capacity biodiesel production facilities have the resources to employ additional unit operations, such as energy-intensive distillation processes, to recover methanol from their waste glycerol (Figure 1, pink). Reuse of the recovered methanol recycled from the waste glycerol streams decreases the net operation cost of biodiesel production. Additionally, their higher-purity glycerol can be sold at ~\$0.30/kg, an order of magnitude higher price than CG. This approach proves cost-effective at higher production volumes due to economies of scale. The resulting waste glycerol stream has a higher glycerol (80–85%) and lower methanol (1%) content. Henceforth, we refer to this *methanol-lean waste glycerol*, with the additional methanol recovery steps seen primarily in high-capacity facilities, as “*methanol-depleted crude glycerol*” (MD-CG).

Formulation and Characterization of Synthetic Waste Glycerol.

To effectively evaluate electrocatalytic processes for both crude glycerol (CG) and methanol-depleted crude glycerol (MD-CG), we selected one representative composition from each range based on our collected primary data (Figure 1b, dashed lines). Synthetic CG, modeled after low-capacity facilities, contains 50.0% glycerol (6.2 M), 22.5% methanol (8.1 M), 5.0% NaOH (1.5 M), and 22.5% water by weight, while synthetic MD-CG, modeled after high-capacity facilities, contains 80% glycerol (11.0 M), 0.1% methanol (0.04 M), 6.0% NaOH (1.9 M), and 14.0% water by weight (Table S2). These compositions are notable for their extreme concentrations of glycerol, well beyond that typically used in studies of the electrooxidation of purified glycerol (0.1–1.0 M).^{48,49} In addition, the concentration of methanol in CG is 1.9 M greater than that of glycerol. Interestingly, the concentrations of NaOH are comparable (1.5 M vs 1.9 M). To pursue integrated biodiesel production with economic enhancement from electrooxidative valorization of its major byproduct stream, we tested these compositions in electrolysis experiments.

To further approximate industrial operating conditions, we utilized a flow electrolyzer in single-pass mode with scalable gas diffusion electrodes as described in previous work.^{50–52} Flowing liquid electrolyte streams at both the cathode and the anode are fed through a flow field comprising submillimeter-wide channels. The resistance of these channels imposes a limit on the maximum viscosity of the electrolyte. The glycerol concentrations in both CG and MD-CG imparted viscosities close to or exceeding our operational limit (Figure 1b, inset, black line; Table S2). Thus, we investigated the viscosities of adjusted compositions of CG (Figure 1b, inset, green curve) and MD-CG (Figure 1b, inset, pink curve) by adding water and/or aqueous (NaOH). Unadjusted CG met the viscosity criterion, while MD-CG required a 0.33-to-1 mass dilution (i.e., addition of 0.33 g water for every 1 g crude) to do so. Rheological characterization of these solutions (Figure S16) and further electrochemical testing of the resulting anolyte solutions (Figures S1–S2 and Supporting Text S3) indicated that electrochemical activity is limited by mass transport owing to anolyte viscosity (vide infra). Notably, variations in current density do not correlate with product concentrations. This was evidenced by unadjusted CG, which, despite having the lowest current density of all the tests at -24 mA/cm^2 , also showed the highest total concentration of formate at 9.0 mM (Figures S1–S2). Comparison of dilutions also indicated that, despite

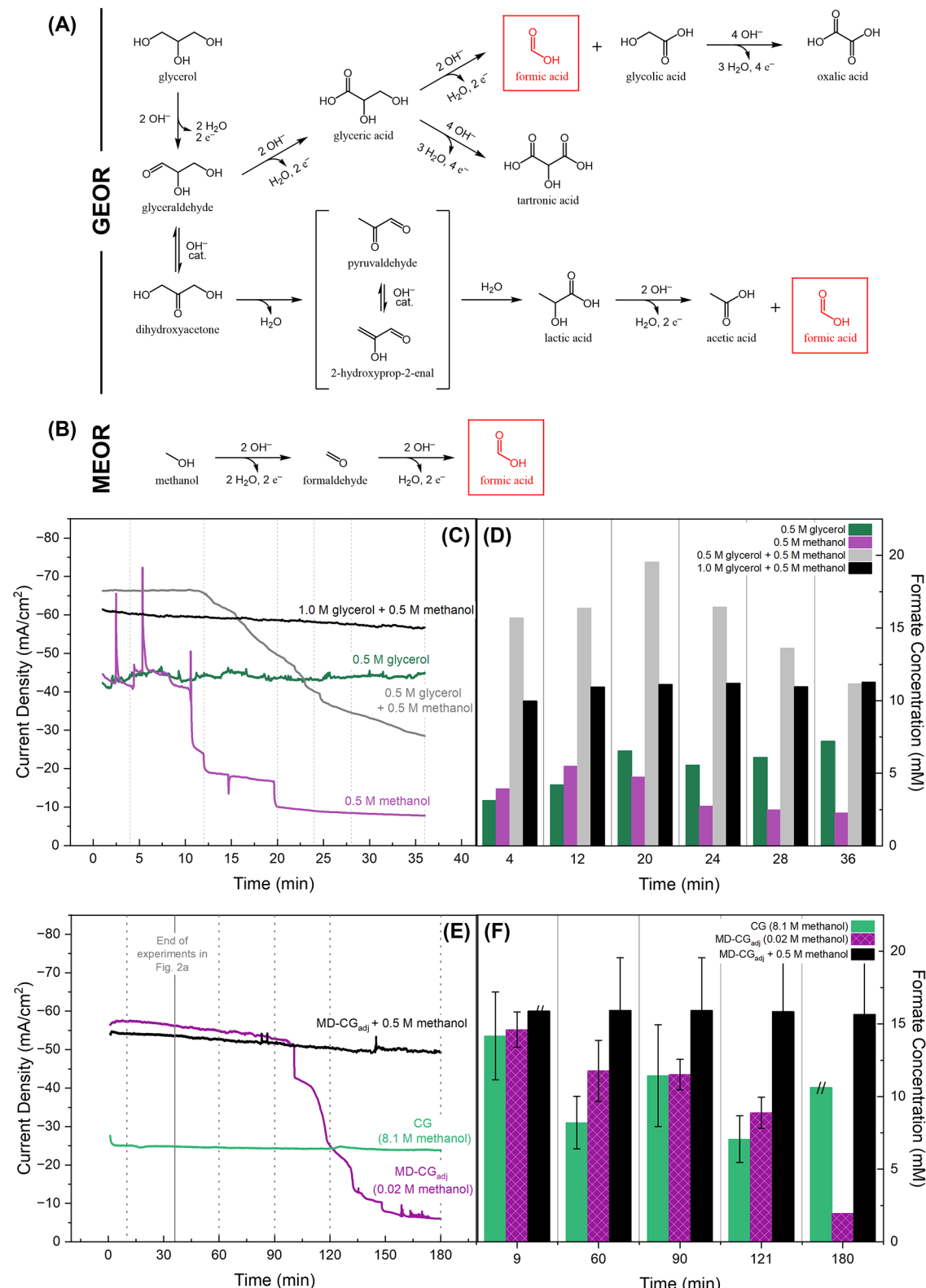


Figure 2. Reaction schemes for (A) glycerol electrooxidation and (B) methanol electrooxidation, highlighting formic acid as a shared product between three possible oxidative pathways. (C) Current densities and (D) formate concentrations measured over 36 min chronoamperometric experiments at -1.5 V cell potential, demonstrating the variations in performance of 0.5 M glycerol electrooxidation (green), 0.5 M methanol electrooxidation (purple), 0.5 M glycerol + 0.5 M methanol electrooxidation (gray), and 1.0 M glycerol + 0.5 M methanol (black). Anodic potentials for these experiments vary by 41 mV or less (Table S4), indicating performance is directly comparable. GEOR performance (both current density and formate production) is generally stable over time, while MEOR performance degrades over time (spikes in current are due to bubble formation in the reactor channel). The simulated crude of 0.5+ 0.5 starts with 1.5 \times current density and 2.5 \times formate production than the individual reactions, but both metrics decline over time. The degradation pattern appears remarkably like attenuated MEOR performance. While the system with 0.5 M glycerol mimics the passivating behavior of MEOR, adding more glycerol (1.0 M) appears to stabilize both current density and formate production.

Figure 2. continued

(E) Current densities and (F) formate concentrations of CG, MD-CG_{adj}, and MD-CG_{adj} with 0.5 M methanol. CG, at over 8 M methanol, shows stable performance for 3 h. MD-CG_{adj}, with less than 0.1 M methanol, decays after just over an hour and a half of operation. However, the same composition of MD-CG_{adj} with 0.5 M methanol does not show the same dramatic decay. This confirms that higher concentrations of glycerol will indeed stabilize performance in the presence of low concentrations of methanol; however, this stabilization is temporary, and the current density will eventually decay. Increasing the concentration of methanol in the presence of high glycerol concentrations increases the stability of the electrolysis process over long-term operation.

current densities up to 38% higher, product concentrations decreased up to 34% with increasing dilution (Figures S1a,b and S2a,b). Exploring the effect of increasing concentration of NaOH indicated that maximum product concentrations were achieved with unadjusted CG, while comparable product concentrations from MD-CG required both 1-to-1 mass dilution and further addition of NaOH (Figure S2c,d).

While activity loss, i.e., a decrease in current density, remains a reasonable metric to evaluate catalyst deactivation, the common interpretation of current density as proportionate to product generation does not apply here. Changing the viscosity and amount of analyte in the anolyte stream changes the conductivity and therefore the resistance of the electrolyte, which directly impacts the resultant current density (Section S3). To evaluate whether this relationship held true in our system, we undertook several analyses. First, we compared cyclic voltammograms of the different synthetic waste glycerol streams (Figure S22). While these cyclic voltammograms appear to show a reduction in overall reaction rate due to the shift from higher currents using MD-CG_{adj} to lower currents using CG, it is important to note that the conductivity of CG is 4 times lower than that of MD-CG_{adj}, and yet the production rate of CG is 1.6 times that of MD-CG_{adj} (Tables S2–S3). It can furthermore be seen that the voltage at which peak alcohol oxidation current occurs is shifted 30 mV higher for CG and ISG_{adj} relative to MD-CG_{adj}, which typically indicates resistance-related phenomena. Notably, our operating half-cell voltages for chronoamperometric testing of synthetic waste glycerol did not vary significantly, with standard deviations of 13 mV (anode) or 23 mV (cathode; Table S4). These data demonstrate that the shift in voltammetry is not necessarily an intrinsic function of reaction rate, but instead a systematic change in the physical properties of the analytes used.

Because the objective in the electrooxidative conversion of waste glycerol is to maximize profits (i.e., produce meaningful amounts of a value-added product while minimizing associated costs from dilution, purification, etc.), we made two key decisions. First, we used the streams which generated the highest formate concentrations at the highest production rates, regardless of current density: (1) *unadjusted CG* and (2) *compositionally adjusted MD-CG* (MD-CG_{adj}, 4.9 M glycerol, 0.02 M methanol), prepared by diluting 1-to-1 by mass with water to adjust the viscosity and compensating the reduction in conductivity by restoring the NaOH concentration to 1.5 M (as in unadjusted CG). Second, we utilized a constant applied voltage across the entire electrolyzer, i.e., a two-electrode operating configuration. A two-electrode operating configuration mimics reactor operating conditions used in scaled membrane electrode assembly electrolyzers and therefore provides a more realistic benchmark for operation in a manufacturing facility. An operating voltage of −1.5 V was selected, as it fell in between the oxidation peaks of the different streams, as shown by cyclic voltammetry (Figure S22).

Interplay between Electrolysis of Methanol and Glycerol in Synthetic Waste Glycerol. Our initial testing of the electrooxidation of unmodified and modified synthetic waste glycerol feeds on a nickel catalyst indicated that our system shows repeatable robustness to compositional changes (Figure S5). However, while nickel electrodes are generally resistant to CO poisoning,^{27,32,33} prior work has also shown that Ni electrodes can be deactivated by concentrations of methanol at or below 0.5 M.²⁶ Because MD-CG_{adj} has a “low” methanol concentration of 0.02 M, we endeavored to ascertain the impacts of methanol concentration on electrooxidative performance by comparing two model feeds: 0.5 M methanol + 1 M NaOH (methanol electrooxidation reaction, MEOR) and 0.5 M glycerol + 1 M NaOH (glycerol electrooxidation reaction, GEOR). Per the reaction pathways reported previously,^{26,27} both MEOR and GEOR can produce the target value-added product formate; indeed, GEOR can produce formate from two divergent reaction pathways (Figure 2a,b). We tested these feeds at −1.5 V cell potential, which gave consistent half-cell voltages and maximized product concentration as compared to a higher applied cell voltage of −1.9 V (Table S4 and Figures S1–S2e,f). While the current density and formate concentration from GEOR typically did not vary (Figure 2c,d, green), a 77% reduction in current density and a 51% reduction in formate production was observed during MEOR from 8 to 20 min (Figure 2c,d, purple). We attribute this performance discrepancy to mechanism. While GEOR follows an indirect mechanism that is agnostic to concentration (Scheme S1a),²⁷ MEOR follows a direct, concentration-dependent mechanism (Scheme S1b–c),²⁶ which permits potentially deactivating (hydro)-peroxy species to accumulate on the catalyst surface at concentrations of methanol at or below 0.5 M. Similarly, when oxidizing a mixture of 0.5 M methanol and 0.5 M glycerol, current density and formate production are, respectively, 1.5 times and 2.5 times those attained using the individual analytes (Figure 2c,d, gray), indicating that GEOR and MEOR are both occurring. This was confirmed by both NMR and HPLC analysis, which identified multiple glycerol electrooxidation products (e.g., glycolate), as well as the specific coproducts of formate production from GEOR (lactate, acetate; Figures 2a, and S17–S20 and S24a). However, both current density and formate production began declining at the same time as was observed for MEOR alone. This observation suggests that the presence of 0.5 M methanol still leads to the aforementioned catalyst deactivation.

Curiously, when we increased the amount of glycerol to 1.0 M, formate concentrations remained stable at 11 mM throughout the 36 min experiment, with only 7 mA/cm² of current density decay (Figure 2c,d, black). This surprising result, which we confirmed was not due to the ratio of methanol to glycerol (Figure S3), indicates that the increased glycerol concentration stabilizes the nickel surface, despite the catalyst deactivation observed for 0.5 M methanol alone.

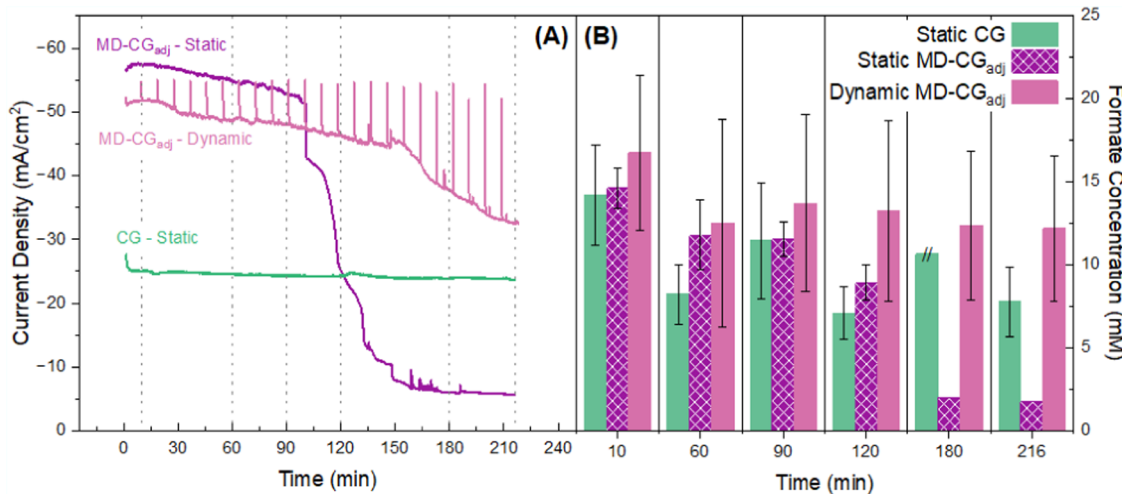


Figure 3. (A) Current density and (B) formate concentration for 3.6-h tests of CG and MD-CG_{adj}, using a static chronoamperometric hold at -1.5 V cell potential, as well as a 3.6-h test of MD-CG_{adj} using a dynamic operating protocol (9 min of operation at -1.5 V followed by 5 s of operation at 0 V cell potential). CG remains stable for the full operation time using the static protocol, producing around 10 mM of formate, whereas the performance of MD-CG_{adj} in the static protocol decays after approximately halfway through the operation time. The dynamic protocol used for MD-CG_{adj} leverages a 5-s pulse every 9 min to refresh the catalyst, increasing current density stability by $1.25\times$ and enabling production of around 12.5 mM formate for the full operation time. Note that the full pulse (which goes down to 0 mA/cm^2) has been hidden for visual clarity; the reader can find the complete data shape in Figures S13–S14.

Comparison of cyclic voltammograms before and after electrolysis indicated that, when “deactivated” chronoamperometrically, the catalysts are still usable, but only for the oxygen evolution reaction (OER; Figure S23). For (0.5 M methanol) and (0.5 M glycerol + 0.5 M methanol), OER after electrolysis shows the same onset potential as the alcohol electrooxidations seen pre-electrolysis (Figure S23c). It is possible that increasing glycerol concentration, which have been shown to delay the onset of OER by reducing OER-active nickel(II) (hydro)peroxide hydroxide species to nickel(II) hydroxide,^{49,53,54} may reduce some of the (hydro)peroxyl species formed in the electrooxidation of methanol concentrations ≤ 0.5 M, prolonging catalytic activity in a dynamic interplay.

To ascertain whether this surprising finding would hold true for waste glycerol, we tested CG (green curve), MD-CG_{adj} (purple curve) and MD-CG_{adj} with additional methanol (0.5 M methanol, 4.9 M glycerol; black curve) (Figure 2e,f). Remarkably, in line with our surprising observation, CG remained stable for over 210 min. On the other hand, despite stable performance for longer than the 36 min experiments in Figure 2c, both current density and formate concentration of MD-CG_{adj} decayed after approximately 100 min of electrolysis. Increasing the concentration of methanol in MD-CG_{adj} to 0.5 M eliminated the decline in performance. This result indicates that elevated glycerol concentrations will delay the onset of surface deactivation, but in the presence of methanol concentrations less than 0.5 M, (hydro)peroxyl species on the surface will eventually accumulate and degrade performance (Scheme S1c).

While a comprehensive mechanistic analysis of the interplay between GEOR and MEOR in these waste glycerol streams is beyond the scope of this work, we surmise that, at concentrations of methanol ≤ 0.5 M, increasing the concentration of glycerol delays the formation of (hydro)peroxyl species on the catalyst surface, suppressing immediate deactivation and the corresponding activity loss.

Electrolysis of Synthetic Waste Glycerol. Next, we tested the electrooxidation of CG and MD-CG_{adj} in longer electrolysis experiments (3.6-h static chronoamperometry) to

unravel the effects of synthetic waste glycerol electrooxidation over time (Figure 3). As expected from their differences in conductivity (vide supra), initial current densities of MD-CG_{adj} (purple curve) were 1.8 times those of CG (green curve). Intriguingly, the current density of CG remained stable throughout the experiment, losing less than 4 mA/cm^2 (14% loss over 3.6 h), accompanied by no observable decay in formate production. On the other hand, the activity of MD-CG_{adj} decayed rapidly approximately halfway through the experiment, losing over 50 mA/cm^2 (90% decay over 3.6 h) and, with that, almost all formate production. Notably, half-cell potentials for these experiments are nearly invariant (standard deviation 13 mV (anodic) and 60 mV (cathodic); Table S4), allowing for direct comparison of the performance of these complex reactant streams. Because glycerol has been shown to perform well on an aged nickel surface,⁵⁵ we hypothesize that the observed activity loss corresponds to methanol-induced catalytic surface deactivation (vide supra).

To prevent extensive deactivation during electrolysis of MD-CG_{adj}, we employed a *dynamic operation protocol* inspired by the work of Kormányos, Janáky, and co-workers on GEOR⁵⁶ and other works on different chemistries.^{39,57,58} These protocols are almost exclusively used to reactivate noble metal catalysts poisoned by oxidation. Our protocol uses a five-second pulse at 0 V cell potential after 9 min of electrolysis to reactivate the electrode (Figure S4). The process of reactivation is likely similar to the mechanisms described in the literature (vide supra), where the catalyst surface is reduced during the “pulse” step. We hypothesize that this reduces deactivating species from the Ni catalyst surface, enabling longer-term operation.

While the dynamic protocol did not completely prevent activity loss, it dramatically improved both current density stability and formate production rates (Figure 3, pink curve). The rate of activity loss is far less severe than without the dynamic protocol, resulting in a loss of only 7 mA/cm^2 over the first 2.5 h (14% loss, identical to that of CG). Even with the onset of decay rates greater than 1 $\text{mA}/\text{cm}^2 \text{ min}$ after 2.5 h

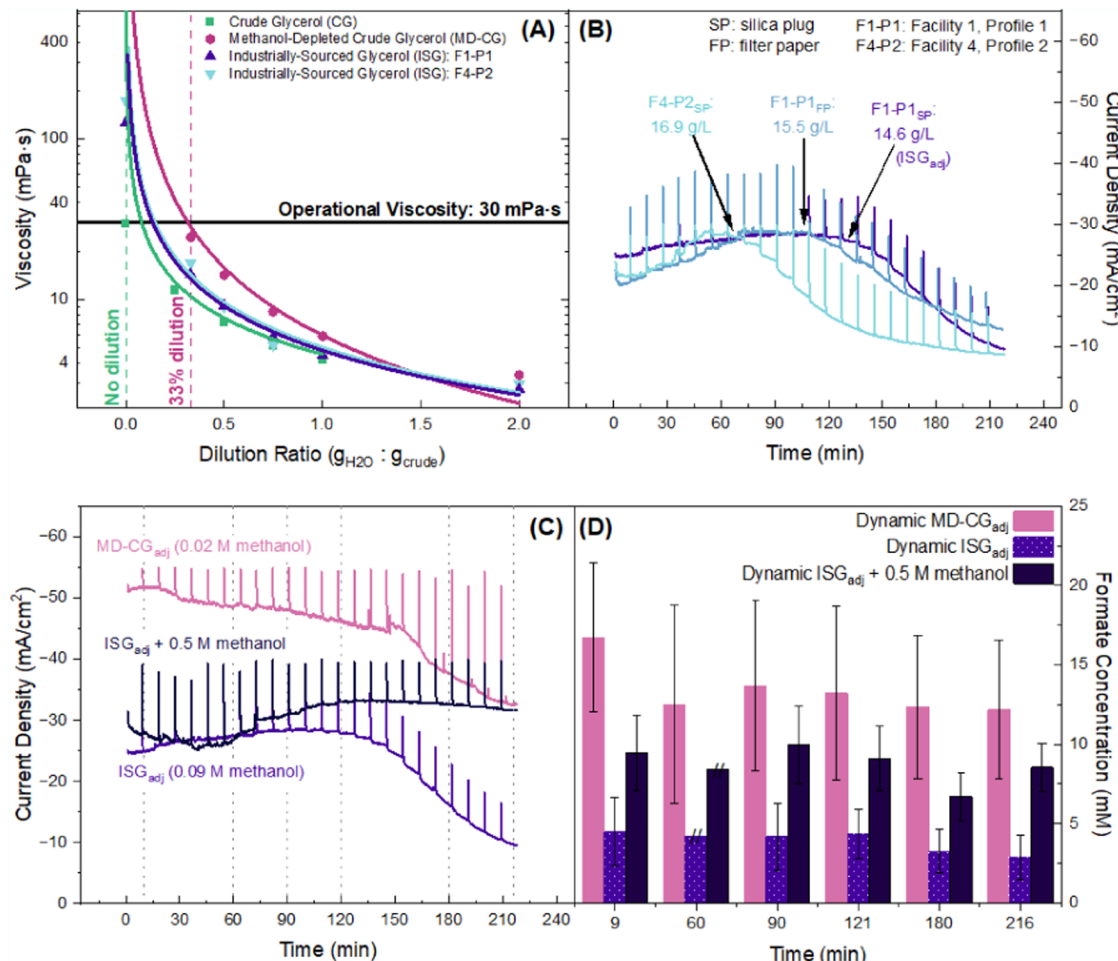


Figure 4. (A) Comparison of dilution ratio versus viscosity for CG, MD-CG, and ISG from two industrial sources. The viscosities of ISG from F1–P1 and F4–P2 are nearly identical and comparable to the profiles of CG and MD-CG. (B) Comparison of the chronoamperometric performance of MD-CG-type, industrially sourced waste glycerol (ISG) streams with different amounts of impurities using the dynamic operating protocol described in Figure 3. As the concentration of impurities increases, the onset of activity decay is earlier, and the increase in current density preceding decay is more pronounced. We chose to use the F1–P1_{SP} for further testing as ISG_{adj}. (C) Current density and (D) formate concentration for 3.6-h tests of ISG_{adj} with and without 0.5 M methanol, and comparison to MD-CG_{adj}. However, the patterns in the current and formate concentrations—including the onset of degradation at approximately 150 min—are nearly identical. This is further demonstrated by the stabilization of ISG_{adj} with the addition of 0.5 M methanol.

(Figure S7), overall activity loss remains under 20 mA/cm² (38%), in contrast to 90% loss using the static protocol. Our results bear similarities to other long-term experiments leveraging dynamic operating conditions, which demonstrate a meaningful extension of the reaction lifetime.⁵⁹ While our results at different pulse frequencies show no meaningful performance improvements for MD-CG_{adj} electrolysis (Figure S14), the protocol could be further optimized and improved to achieve multihour stability. Further investigation will be necessary to identify the exact nature of the processes underlying the remaining activity loss.

Based on our evaluation of the interplay between GEOR and MEOR (vide supra, Figure 2), we posit that the 0.02 M concentration of methanol in MD-CG_{adj} is the source of performance loss over time, even at high glycerol concentration. On the other hand, the high concentration of methanol in CG, paired with the high concentration of glycerol, seem to enable stable operation without the need for electrode reactivation.

Electrolysis of Industrially-Sourced Waste Glycerol.

Having successfully established the key operating parameters

for stable long-term synthetic waste glycerol electrooxidation, we applied these lessons to *industrially sourced waste glycerol* (ISG). After obtaining MD-CG-type waste glycerol from two unique industrial sources (Facility 1-Profile 1, F1–P1 and Facility 4-Profile 2, F4–P2; Table S1), we evaluated their rheological properties. Both streams demonstrated similar rheological properties to MD-CG and nearly identical properties to each other (Figure 4a, purple and light blue curves). After physical removal of phase-separated oily fractions, we filtered the crude ISG samples using either silica plugs (SP) or filter paper (FP) to remove residual triglycerides from the biodiesel synthesis processes (Supporting Text S2 and Figures S8–S9, vide infra). We then adjusted the ISG compositions by dilution and NaOH addition (as before for synthetic MD-CG) to prepare ISG_{adj}. Leveraging the dynamic operating protocol established for synthetic MD-CG_{adj}, we demonstrated stable electrolysis of these samples for 1.0 to 2.5 h, after which activity loss of 43% (F1–P1_{FP}) to 66% (F4–P2_{SP}) occurred (Figure 4b). While the dynamic operating protocol at the 9 min pulse interval meaningfully improved

performance vs slower pulsing or static chronoamperometry (Figure S10), the source of activity loss remained unclear.

Taking another lesson from our study of synthetic waste glycerol, we sought to understand whether increasing the methanol content in ISG_{adj} would mitigate the observed activity loss. Utilizing F1–P1_{SP} as a stable representative ISG_{adj}, we added 0.5 M methanol to the feed to ensure we met the 0.5 M threshold established in our study of synthetic waste glycerol (*vide supra*). Remarkably, formate production stabilized, and current density, in fact, improved and stabilized after the first 60 min (Figure 4c).

After reproducing these results (Figure S13), we endeavored to disentangle the effects of methanol concentration from those of triglyceride impurities present in the ISG_{adj} feed. To do so, we back-calculated the concentration of triglycerides present in each ISG_{adj} stream (Supporting Text S2) and qualitatively confirmed those calculations by comparing the color of each stream (Figure S9). By comparing multiple filtered ISG_{adj} profiles as a function of their approximate triglyceride concentrations, the influence of triglyceride concentration became apparent (Figure 4b). Triglyceride concentration depends on both the ISG source (F4–P2_{SP} has 14% more triglycerides F1–P1_{SP}) and the filtration method (F1–P1_{SP} has 6% less triglycerides than F1–P1_{FP}). Although activity decreases for all ISG_{adj} (as triglyceride concentrations increase), the onset of activity loss occurs earlier and the “peaks” preceding onset become more acute. In other words, a period of activity gain is followed by activity loss.

Because adding methanol to ISG_{adj} stabilizes performance, these results ostensibly indicate that the triglycerides present in the feed stream initially block active catalyst sites. By periodically restoring the catalyst surface using the dynamic operating protocol, the triglycerides are removed, leading to an increase in adsorption of both methanol and glycerol on the active sites and the observed activity gain. Increasing concentration of triglycerides in the feed stream makes the resultant activity gain more acute. However, the concentration of methanol \leq 0.5 M in the feed stream leads to the accumulation of (hydro)peroxyl species on the catalyst surface (*vide supra*), which in turn gradually deactivates the catalyst and leads to the observed activity loss. Of course, some of these low-methanol-concentration-related performance issues can be avoided by leaving methanol in the ISG to begin with.

In sum, the dynamic protocol prolongs operating time before activity losses but cannot fully overcome the effects of feed stream composition. Higher concentration of triglycerides in the feed stream leads to earlier *onset* of catalytic deactivation, whereas low concentration of methanol in the feed stream is the ultimate *driver* of catalytic deactivation and corresponding activity loss. These results illuminate opportunities for additional studies of catalyst optimization, reactor design, system operation, and process control that could further reduce or eliminate the sensitivity of the waste glycerol electrooxidation system to the concentration of methanol in the feed.

CONCLUSIONS

We demonstrate the electrooxidation of waste glycerol using a scalable system, a low-cost catalyst, and both synthetic- and industrially sourced electrolyzer feeds. First studying the characteristics and challenges of synthetic waste glycerol feeds provided us guidance on how to successfully take on

the challenge of electrooxidative valorization of industrially sourced waste glycerol.

More specifically, we report the engineering of the electrooxidation of waste glycerol feeds of varying compositions and from different biodiesel manufacturing facilities. We demonstrate the intricate interplay between methanol and glycerol concentration *vis à vis* retaining catalyst activity and product speciation. We also demonstrate stable performance in a scalable flow electrolyzer, producing one major product (formate) to minimize separations costs while eliminating the need for extensive reactant purification and the use of PGM catalysts. The experiments detailed in this work reveal that, using a nickel catalyst and a dynamic operating protocol, electrolytic performance critically depends on the presence of a minimum methanol concentration with triglyceride impurities only accelerating the onset of catalytic surface deactivation. In fact, we transformed a mitigating factor (the presence of methanol and its deleterious effect on PGM catalysts) into a beneficial coreactant that both enhances formate production and prevents severe performance degradation.

We describe a method for valorizing waste glycerol streams from both low- and high-capacity biodiesel production facilities. While the waste glycerol streams from low-capacity facilities do not require adjustment, electrooxidative valorization of waste glycerol streams at high-capacity facilities (MD-CG) requires both compositional adjustments and a dynamic operating protocol—the combination of which still does not fully eliminate the activity and product speciation losses resulting from low feed concentrations of methanol. Tailoring pre-electrolysis treatment steps such as filtration, which we used in this work, and fine-tuning the interplay between reactor-, reaction-, and catalyst engineering could enhance the feasibility of waste glycerol electrooxidation in scaled operations.

Omission of resource-intensive glycerol purification steps could also improve efficiency. Detailed technoeconomic analysis and life cycle assessment of the presented approaches using comprehensive mass and energy balances in scaled electrolysis configurations that maximize formate productivity and purity, provide further insight into the economic opportunity for valorizing industrially sourced waste glycerol. We present the results of this analysis in a separate study.⁶⁰

In general, this study shows that a holistic analysis of the composition of a crude feed can reveal key insights into the feasibility of using those crude feeds in a more economically feasible fashion.

MATERIALS AND METHODS

Primary Data Collection from U.S. Biodiesel Producers. Existing U.S. biodiesel facility and production data were obtained from the U.S. Energy Information Administration (EIA) database, which includes publicly available data on biodiesel producer company names, locations, and production capacity.⁶¹ We contacted all 77 U.S. production facilities reported in 2022 EIA data via an email questionnaire and follow-up phone calls (Supporting Text S1). Of these 77 facilities, we received responses from 19 facilities (24.6% response rate) providing detailed waste glycerol profiles. Some large biodiesel producers provided the composition profiles of multiple waste glycerol products, for a total of 22 waste glycerol profiles.

Flow Electrolysis System Setup. Electrolysis was performed in a benchtop-scale flow electrolyzer, as described in previous work.^{50,51,58,62,63} Briefly, the electrolyzer is comprised of two stainless-steel current collectors containing gas flow chambers. Electrocatalysts separated the gas flow chamber from the two

electrolyte flow chambers made of inert polyether ether ketone. Electrocatalysts were prepared by sputtering Ni (anode, 0.6 ± 0.06 mg/cm²) or Pt (cathode, 0.65 ± 0.065 mg/cm²) onto gas diffusion electrodes (Freudenberg H23C6, Fuel Cell Store) using a sputtering system with DC argon plasma (Orion 3, AJA). The geometric area of each electrode was 1 cm².

The electrolyte flow chambers were separated by an anion exchange membrane (Fumasep Fumion FAA-PK-75, Fuel Cell Store) to minimize crossover. During operation, the flow rate was held at 0.5 mL/min to prevent GDE failure for compositions with the highest viscosities. Catholyte was 1 M NaOH for all operational conditions. Anolyte was composed of NaOH (Ward's Science, reagent grade), glycerol (Fisher Chemical, certified ACS), and methanol (Fisher Chemical, certified ACS), with concentrations as described above.

All experiments were performed in single-pass mode and tested by applying a constant cell potential of -1.5 V across the full electrolyzer. Potentials are reported without *iR* compensation.

Waste Glycerol Preparation. MD-CG-type waste glycerol was obtained from Facility 1 and Facility 4. The waste glycerol was prepared using 1:1 dilution, filtration through qualitative filter paper or silica plug, addition of 1.5 M NaOH and, where relevant, 0.5 M methanol (Figures S8–S9).

Rheological Characterization of Waste Glycerol. The viscosity of waste glycerol formulations was measured on a stress-controlled MCR 302 Rheometer (Anton Paar) using a double-gap Couette cell. A shear rate ramp was performed from 10 to 1000 s⁻¹, in 30 s increments. The viscosity was then calculated by dividing the steady-state shear stress by the applied shear rate. The viscosity was independent of shear rate, and the reported values in Figure 1 were calculated at 100 s⁻¹.

Pre-Electrolysis Cyclic Voltammetry. Prior to each electrolysis reported in this work, we performed a series of cyclic voltammetry (CV) sweeps to confirm, condition, and characterize the electrode surface (Figure S21). These sweeps were performed in the electrolyte used for the subsequent chronoamperometry tests. First, we performed 1 cycle of CV from -0.3 to -2.5 V cell potential at 50 mV/s to confirm the system was operating correctly. Second, we performed 5 cycles of CV from -0.3 to -2.5 V cell potential at 100 mV/s to condition the surface of the electrode. Third, we performed 1 cycle of CV from -0.3 to -2.1 V cell potential at 10 mV/s to characterize the electrode. After this voltammetric sequence, we commenced chronoamperometric tests.

Product Collection. Product samples were collected for 2 min, with reported times being the end points of each collection unless otherwise noted. 0.5 mL of each sample was immediately acidified with 0.5 mL of 0.5 M H₂SO₄ (Sigma-Aldrich, ACS reagent, 95.0–98.0%) and stored for HPLC analysis. To account for electrolyte decomposition, prior to experimentation, 0.5 mL of unused anolyte was collected and acidified. This solution baseline composition was subtracted from subsequent samples taken during electrolysis.

Data Analysis. Analysis of products was performed using a MATLAB script as described in our previous work;⁵⁰ the script is available online.⁶⁴ Because of the high complexity of the electrolytes, not every product sample converged using the script nor using manual integration. To evaluate these time points, averages were taken using the time point preceding and following each sample. These averaged product concentrations are marked with hash marks instead of error bars in the representative figures. Because of peak splitting and overlapping of glycerol and formate peaks in many chromatograms, deconvolution was difficult (Figures S12 and S24 give representative examples). Thus, error bars for individual samples represent the mean of the total possible variation in the amount of formate measured in each sample. To qualitatively confirm product distributions were as expected, we utilized NMR on select samples (Figures S17–S20).

ASSOCIATED CONTENT

Supporting Information

The Supporting Information is available free of charge at <https://pubs.acs.org/doi/10.1021/acssuschemeng.Sc03028>.

Additional experimental details, materials, and methods, including photographs of filtration setup; supporting data for electrolysis experiments, viscosity tests, and compositional analysis; complete data tables for waste glycerol compositions; reaction schemes; ¹H NMR and HPLC spectra (PDF)

AUTHOR INFORMATION

Corresponding Author

Paul J. A. Kenis – Department of Chemical and Biomolecular Engineering, University of Illinois Urbana-Champaign, Urbana, Illinois 61801, United States;  orcid.org/0000-0001-7348-0381; Email: kenis@illinois.edu

Authors

Rachel N. Gaines – Department of Chemical and Biomolecular Engineering, University of Illinois Urbana-Champaign, Urbana, Illinois 61801, United States;  orcid.org/0000-0003-1953-0194

Adam P. Sibal – Department of Civil and Environmental Engineering, University of Illinois Urbana-Champaign, Urbana, Illinois 61801, United States;  orcid.org/0002-9786-2410

Abiela M. Bradley – Department of Chemical and Biomolecular Engineering, University of Illinois Urbana-Champaign, Urbana, Illinois 61801, United States;  orcid.org/0000-0001-8075-1936

James J. Griebler – Department of Chemical and Biomolecular Engineering, University of Illinois Urbana-Champaign, Urbana, Illinois 61801, United States;  orcid.org/0000-0002-1056-4593

Vijay M. Shah – Department of Chemical and Biomolecular Engineering, University of Illinois Urbana-Champaign, Urbana, Illinois 61801, United States;  orcid.org/0003-2098-3174

Bridget E. Friel – Department of Chemical and Biomolecular Engineering, University of Illinois Urbana-Champaign, Urbana, Illinois 61801, United States

Simon A. Rogers – Department of Chemical and Biomolecular Engineering, University of Illinois Urbana-Champaign, Urbana, Illinois 61801, United States;  orcid.org/0000-0002-3432-5044

Ashlynn S. Stillwell – Department of Civil and Environmental Engineering, University of Illinois Urbana-Champaign, Urbana, Illinois 61801, United States;  orcid.org/0002-6781-6480

Complete contact information is available at:

<https://pubs.acs.org/10.1021/acssuschemeng.Sc03028>

Author Contributions

Conceptualization: R.N.G., A.P.S., A.S.S., P.J.A.K. Methodology: R.N.G., A.M.B. Investigation: R.N.G., A.P.S., A.M.B., J.J.G., V.M.S., B.E.F. Data curation: R.N.G., J.J.G. Visualization: R.N.G., V.M.S. Writing—original draft: R.N.G., P.J.A.K. Writing—review and editing: R.N.G., A.P.S., A.M.B., J.J.G., V.M.S., B.E.F., S.A.R., A.S.S., P.J.A.K. Supervision: S.A.R., A.S.S., P.J.A.K. Funding Acquisition: S.A.R., A.S.S., P.J.A.K.

Notes

The authors declare no competing financial interest.

ACKNOWLEDGMENTS

The authors gratefully acknowledge the contributions of Dr. Dean Olson of the UIUC NMR Lab and Ms. Dorothy Loudermilk of the UIUC Graphic Services team. RNG, APS, BEF, ASS, and PJAK acknowledge funding from the National Science Foundation EFRI-DCeM grant 2029326; RNG, AMB, and PJAK acknowledge funding from the National Science Foundation FMRG-Cyber grant 2328160; RNG acknowledges a TechnipFMC Foundation grant. The team acknowledges the National Science Foundation grant DMR-2309037 for support in catalyst fabrication and evaluation.

REFERENCES

- (1) Rezania, S.; Oryani, B.; Park, J.; Hashemi, B.; Yadav, K. K.; Kwon, E. E.; Hur, J.; Cho, J. Review on Transesterification of Non-Edible Sources for Biodiesel Production with a Focus on Economic Aspects, Fuel Properties and by-Product Applications. *Energy Convers. Manage.* **2019**, *201*, No. 112155.
- (2) Anuar, M. R.; Abdullah, A. Z. Challenges in Biodiesel Industry with Regards to Feedstock, Environmental, Social and Sustainability Issues: A Critical Review. *Renewable Sustainable Energy Rev.* **2016**, *58*, 208–223.
- (3) Ayoub, M.; Abdullah, A. Z. Critical Review on the Current Scenario and Significance of Crude Glycerol Resulting from Biodiesel Industry towards More Sustainable Renewable Energy Industry. *Renewable Sustainable Energy Rev.* **2012**, *16* (5), 2671–2686.
- (4) Dodekatos, G.; Schünemann, S.; Tüysüz, H. Recent Advances in Thermo-, Photo-, and Electrocatalytic Glycerol Oxidation. *ACS Catal.* **2018**, *8* (7), 6301–6333.
- (5) Johnson, D. T.; Taconi, K. A. The Glycerin Glut: Options for the Value-Added Conversion of Crude Glycerol Resulting from Biodiesel Production. *Environ. Prog.* **2007**, *26* (4), 338–348.
- (6) Luo, H.; Barrio, J.; Sunny, N.; et al. Progress and Perspectives in Photo- and Electrochemical-Oxidation of Biomass for Sustainable Chemicals and Hydrogen Production. *Adv. Energy Mater.* **2021**, *11*, No. 2101180, DOI: 10.1002/aenm.202101180.
- (7) Beltrán-Prieto, J. C.; Kolomazník, K.; Pecha, J. A Review of Catalytic Systems for Glycerol Oxidation: Alternatives for Waste Valorization. *Aust. J. Chem.* **2013**, *66* (5), 511–521.
- (8) Nabil, S. K.; Raghuwan, M. A. M.; Kannimuthu, K.; Rashid, M.; Shiran, H. S.; Kibria, M. G.; Khan, M. A. Acid–Base Chemistry and the Economic Implication of Electrocatalytic Carboxylate Production in Alkaline Electrolytes. *Nat. Catal.* **2024**, *7* (3), 330–337.
- (9) Maya-Cornejo, J.; Guerra-Balcázar, M.; Arjona, N.; Álvarez-Contreras, L.; Rodríguez Valadez, F. J.; Gurrola, M. P.; Ledesma-García, J.; Arriaga, L. G. Electrooxidation of Crude Glycerol as Waste from Biodiesel in a Nanofluidic Fuel Cell Using Cu@Pd/C and Cu@Pt/C. *Fuel* **2016**, *183*, 195–205.
- (10) Frutis-Murillo, M.; Velázquez-Hernández, I.; Esparza, R.; López-Meza, J. E.; Cayetano-Castro, N.; Rosas, G. Facile Synthesis of Gold Nanoflowers and Their Application in Glycerol Electro-Oxidation. *Appl. Surf. Sci.* **2024**, *642*, No. 158628.
- (11) Olivares-Ramírez, J. M.; Dector, A.; Bañuelos-Días, J. A.; Amaya-Cruz, D. M.; Ortiz-Verdín, A.; Jiménez-Sandoval, O.; Sabaté, N.; Esquivel, J. P. Evaluation of a Passive Anion-Exchange Membrane Micro Fuel Cell Using Glycerol from Several Sources. *Fuel Cells* **2019**, *19* (1), 10–18.
- (12) Zhang, Z.; Xin, L.; Qi, J.; Chadderdon, D. J.; Li, W. Supported Pt, Pd and Au Nanoparticle Anode Catalysts for Anion-Exchange Membrane Fuel Cells with Glycerol and Crude Glycerol Fuels. *Appl. Catal., B* **2013**, *136–137*, 29–39.
- (13) Velázquez-Hernández, I.; Estévez, M.; Vergara-Castañeda, H.; Guerra-Balcázar, M.; Álvarez-Contreras, L.; Luna-Bárcenas, G.; Pérez, C.; Arjona, N.; Pool, H. Synthesis and Application of Biogenic Gold Nanomaterials with {1 0 0} Facets for Crude Glycerol Electro-Oxidation. *Fuel* **2020**, *279*, No. 118505.
- (14) Velázquez-Hernández, I.; Zamudio, E.; Rodríguez-Valadez, F. J.; García-Gómez, N. A.; Álvarez-Contreras, L.; Guerra-Balcázar, M.; Arjona, N. Electrochemical Valorization of Crude Glycerol in Alkaline Medium for Energy Conversion Using Pd, Au and PdAu Nanomaterials. *Fuel* **2020**, *262*, No. 116556.
- (15) Velázquez-Hernández, I.; Alvarez-López, A.; Álvarez-Contreras, L.; Guerra-Balcázar, M.; Arjona, N. Electrocatalytic Oxidation of Crude Glycerol from the Biodiesel Production on Pd-M (M = Ir, Ru or Pt) Sub-10 nm Nanomaterials. *Appl. Surf. Sci.* **2021**, *545*, No. 149055.
- (16) Velázquez-Hernández, I.; Torres-Pacheco, L.; Álvarez-López, A.; Álvarez-Contreras, L.; Guerra-Balcázar, M.; Arjona, N. Sustainable Energy Conversion of Crude Glycerol as Biofuel Employing PdBi Nanomaterials. *Appl. Surf. Sci.* **2022**, *602*, No. 154385.
- (17) Arjona, N.; Torres-Pacheco, L. J.; Álvarez-Contreras, L.; Guerra-Balcázar, M. Gold Structures on 3D Carbon Electrodes as Highly Active Nanomaterials for the Clean Energy Conversion of Crude Glycerol. *Electrochim. Acta* **2022**, *430*, No. 141098.
- (18) Hunsom, M.; Saily, P. Electrochemical Conversion of Enriched Crude Glycerol: Effect of Operating Parameters. *Renewable Energy* **2015**, *74*, 227–236.
- (19) Mostafazadeh, A. K.; De La Torre, M. S.; Padilla, Y.; Drogui, P.; Brar, S. K.; Tyagi, R. D.; Le Bihan, Y.; Buelna, G.; Moroyoqui, P. G. An Insight into an Electro-Catalytic Reactor Concept for High Value-Added Production from Crude Glycerol: Optimization, Electrode Passivation, Product Distribution, and Reaction Pathway Identification. *Renewable Energy* **2021**, *172*, 130–144.
- (20) Qi, J.; Xin, L.; Zhang, Z.; Sun, K.; He, H.; Wang, F.; Chadderdon, D.; Qiu, Y.; Liang, C.; Li, W. Surface Dealloyed PtCo Nanoparticles Supported on Carbon Nanotube: Facile Synthesis and Promising Application for Anion Exchange Membrane Direct Crude Glycerol Fuel Cell. *Green Chem.* **2013**, *15* (5), 1133–1137.
- (21) Saily, P.; Hunsom, M. Effect of Additives on One-Pot Electrochemical Conversion of Enriched Crude Glycerol. *Korean J. Chem. Eng.* **2015**, *32* (12), 2412–2417.
- (22) Feng, J.; Wang, X.; Pan, H. In-Situ Reconstruction of Catalyst in Electrocatalysis. *Adv. Mater.* **2024**, *36* (50), No. 2411688.
- (23) Zakari, R. S. B.; Pena, G. D. J. G.; Stephen, S.; Azhagapillai, P.; Delclos, T.; Elsayed, M.; Raj, A.; Hassan Ali, M. I.; Elkadi, M. Crude Bioglycerol Derived Sulfur-Doped Carbon Material for Electro-oxidation of Bioglycerol and Other Alcohols. *Case Stud. Chem. Environ. Eng.* **2024**, *9*, No. 100670.
- (24) Velázquez-Hernández, I.; Olivas, A.; Bañuelos, J. A.; Ramos-Castillo, C. M.; Álvarez-Contreras, L.; Guerra-Balcázar, M.; Arjona, N. Defect Engineering on Metal Oxides (Zn, Mo and Fe) and Their Impact on the Crude Glycerol Biofuel Oxidation. *Int. J. Hydrogen Energy* **2024**, *52*, 1033–1046.
- (25) Schichtl, Z. G.; Conlin, S. K.; Mehrabi, H.; Nielander, A. C.; Coridan, R. H. Characterizing Sustained Solar-to-Hydrogen Electrocatalysis at Low Cell Potentials Enabled by Crude Glycerol Oxidation. *ACS Appl. Energy Mater.* **2022**, *5* (3), 3863–3875.
- (26) Qi, Y.; Zhang, Y.; Yang, L.; Zhao, Y.; Zhu, Y.; Jiang, H.; Li, C. Insights into the Activity of Nickel Boride/Nickel Heterostructures for Efficient Methanol Electrooxidation. *Nat. Commun.* **2022**, *13* (1), No. 4602.
- (27) Goetz, M. K.; Bender, M. T.; Choi, K.-S. Predictive Control of Selective Secondary Alcohol Oxidation of Glycerol on NiOOH. *Nat. Commun.* **2022**, *13* (1), No. 5848.
- (28) Li, Y.; Wei, X.; Chen, L.; Shi, J.; He, M. Nickel-Molybdenum Nitride Nanoplate Electrocatalysts for Concurrent Electrolytic Hydrogen and Formate Productions. *Nat. Commun.* **2019**, *10* (1), No. 5335.
- (29) Houache, M. S. E.; Safari, R.; Nwabara, U. O.; Rafaeleen, T.; Botton, G. A.; Kenis, P. J. A.; Baranton, S.; Coutanceau, C.; Baranova, E. A. Selective Electrooxidation of Glycerol to Formic Acid over Carbon Supported Ni_{1-x}M_x (M = Bi, Pd, and Au) Nanocatalysts and

- Coelectrolysis of CO₂. *ACS Appl. Energy Mater.* **2020**, *3* (9), 8725–8738.
- (30) Rahim, M. A. A.; Hameed, R. M. A.; Khalil, M. W. Nickel as a Catalyst for the Electro-Oxidation of Methanol in Alkaline Medium. *J. Power Sources* **2004**, *134* (2), 160–169.
- (31) El-Shafei, A. A. Electrocatalytic Oxidation of Methanol at a Nickel Hydroxide/Glassy Carbon Modified Electrode in Alkaline Medium. *J. Electroanal. Chem.* **1999**, *471* (2), 89–95.
- (32) Fleischmann, M.; Korinek, K.; Pletcher, D. The Oxidation of Organic Compounds at a Nickel Anode in Alkaline Solution. *J. Electroanal. Chem. Interfacial Electrochem.* **1971**, *31* (1), 39–49.
- (33) Fleischmann, M.; Korinek, K.; Pletcher, D. The Kinetics and Mechanism of the Oxidation of Amines and Alcohols at Oxide-Covered Nickel, Silver, Copper, and Cobalt Electrodes. *J. Chem. Soc., Perkin Trans. 2* **1972**, *0* (10), 1396–1403.
- (34) Dai, C.; Sun, L.; Liao, H.; Khezri, B.; Webster, R. D.; Fisher, A. C.; Xu, Z. J. Electrochemical Production of Lactic Acid from Glycerol Oxidation Catalyzed by AuPt Nanoparticles. *J. Catal.* **2017**, *356*, 14–21.
- (35) Zhang, Z.; Xin, L.; Qi, J.; Wang, Z.; Li, W. Selective Electro-Conversion of Glycerol to Glycolate on Carbon Nanotube Supported Gold Catalyst. *Green Chem.* **2012**, *14* (8), 2150–2152.
- (36) Kwon, Y.; Birdja, Y.; Spanos, I.; Rodriguez, P.; Koper, M. T. M. Highly Selective Electro-Oxidation of Glycerol to Dihydroxyacetone on Platinum in the Presence of Bismuth. *ACS Catal.* **2012**, *2* (5), 759–764.
- (37) Morales, D. M.; Jambrec, D.; Kazakova, M. A.; Braun, M.; Sikdar, N.; Koul, A.; Brix, A. C.; Seisel, S.; Andronescu, C.; Schuhmann, W. Electrocatalytic Conversion of Glycerol to Oxalate on Ni Oxide Nanoparticles-Modified Oxidized Multiwalled Carbon Nanotubes. *ACS Catal.* **2022**, *12* (2), 982–992.
- (38) Zhang, Z.; Xin, L.; Qi, J.; Chadderton, D. J.; Sun, K.; Warsko, K. M.; Li, W. Selective Electro-Oxidation of Glycerol to Tartronate or Mesoxalate on Au Nanoparticle Catalyst via Electrode Potential Tuning in Anion-Exchange Membrane Electro-Catalytic Flow Reactor. *Appl. Catal., B* **2014**, *147*, 871–878.
- (39) Chen, W.; Zhang, L.; Xu, L.; He, Y.; Pang, H.; Wang, S.; Zou, Y. Pulse Potential Mediated Selectivity for the Electrocatalytic Oxidation of Glycerol to Glyceric Acid. *Nat. Commun.* **2024**, *15* (1), No. 2420.
- (40) Thanahiranya, P.; Sadhukhan, J.; Charoensuppanimit, P.; Soottitantawat, A.; Arpornwichanop, A.; Thongchul, N.; Assabumrungrat, S. Sustainability Assessment of Dihydroxyacetone (DHA) Production from Glycerol: A Comparative Study between Biological and Catalytic Oxidation Routes. *ACS Sustainable Chem. Eng.* **2023**, *11* (49), 17425–17439.
- (41) Kim, K.; Jack, J. Delineating Catalyst Deactivation Mechanisms in Electrocatalytic Glycerol Oxidation toward Biodiesel Wastewater/CO₂ Co-Valorization. *Environ. Sci. Technol.* **2025**, *59*, 4388–4398.
- (42) Angizi, S.; Kirici, E. Y.; Higgins, D. Toward Valorization of Crude Glycerol via Controlled Electro-Oxidation. *Trends Chem.* **2024**, *6* (1), 14–21.
- (43) You, B.; Liu, X.; Jiang, N.; Sun, Y. A General Strategy for Decoupled Hydrogen Production from Water Splitting by Integrating Oxidative Biomass Valorization. *J. Am. Chem. Soc.* **2016**, *138* (41), 13639–13646.
- (44) Holade, Y.; Tuleushova, N.; Tingry, S.; Servat, K.; Napporn, T. W.; Guesmi, H.; Cornu, D.; Kokoh, K. B. Recent Advances in the Electrooxidation of Biomass-Based Organic Molecules for Energy, Chemicals and Hydrogen Production. *Catal. Sci. Technol.* **2020**, *10* (10), 3071–3112.
- (45) Luo, H.; Barrio, J.; Sunny, N.; Li, A.; Steier, L.; Shah, N.; Stephens, I. E. L.; Titirici, M.-M. Progress and Perspectives in Photo- and Electrochemical-Oxidation of Biomass for Sustainable Chemicals and Hydrogen Production. *Adv. Energy Mater.* **2021**, *11* (43), No. 2101180.
- (46) Hu, S.; Luo, X.; Wan, C.; Li, Y. Characterization of Crude Glycerol from Biodiesel Plants. *J. Agric. Food Chem.* **2012**, *60* (23), 5915–5921.
- (47) Thompson, J. C.; He, B. B. Characterization of crude glycerol from biodiesel production from multiple feedstocks. *Appl. Eng. Agric.* **2006**, *22* (2), 261–265.
- (48) Simões, M.; Baranton, S.; Coutanceau, C. Electro-Oxidation of Glycerol at Pd Based Nano-Catalysts for an Application in Alkaline Fuel Cells for Chemicals and Energy Cogeneration. *Appl. Catal., B* **2010**, *93* (3), 354–362.
- (49) Oliveira, V. L.; Morais, C.; Servat, K.; Napporn, T. W.; Tremiliosi-Filho, G.; Kokoh, K. B. Studies of the Reaction Products Resulted from Glycerol Electrooxidation on Ni-Based Materials in Alkaline Medium. *Electrochim. Acta* **2014**, *117*, 255–262.
- (50) Gaines, R. N.; Kleimenhagen, B. A.; Griebler, J. J.; Harris, L. C.; Gewirth, A.; Rogers, S. A.; Kenis, P. Optimizing the Flow Electrooxidation of Glycerol Using Statistical Design of Experiments. *J. Electrochem. Soc.* **2024**, *171*, No. 063506.
- (51) Gaines, R. N. Flow Electrolyzers for Reaction Scaling. *Nat. Rev. Clean Technol.* **2025**, *1* (1), No. 12.
- (52) Brösgen, L. Paired Flow Electrosynthesis for Chemical and Hydrogen Co-Production. *Nat. Rev. Clean Technol.* **2025**, *1*, No. 113.
- (53) Oliveira, V. L.; Morais, C.; Servat, K.; Napporn, T. W.; Olivi, P.; Kokoh, K. B.; Tremiliosi-Filho, G. Kinetic Investigations of Glycerol Oxidation Reaction on Ni/C. *Electrocatalysis* **2015**, *6* (5), 447–454.
- (54) Simpson, D. E.; Juda, K. E.; Roy, D. Electroanalytical Assessment of the Function of Nickel in Alkaline Electrocatalysis of Glycerol. *Electrocatalysis* **2018**, *9* (1), 86–101.
- (55) Houache, M. S. E.; Hughes, K.; Safari, R.; Botton, G. A.; Baranova, E. A. Modification of Nickel Surfaces by Bismuth: Effect on Electrochemical Activity and Selectivity toward Glycerol. *ACS Appl. Mater. Interfaces* **2020**, *12* (13), 15095–15107.
- (56) Kormányos, A.; Szirmai, A.; Endrődi, B.; Janáky, C. Stable Operation of Paired CO₂ Reduction/Glycerol Oxidation at High Current Density. *ACS Catal.* **2024**, *14* (9), 6503–6512.
- (57) Zhao, G.; Lin, J.; Lu, M.; Li, L.; Xu, P.; Liu, X.; Chen, L. Potential Cycling Boosts the Electrochemical Conversion of Polyethylene Terephthalate-Derived Alcohol into Valuable Chemicals. *Nat. Commun.* **2024**, *15* (1), No. 8463.
- (58) Cofell, E. R.; Park, Z.; Nwabarwa, U. O.; Harris, L. C.; Bhargava, S. S.; Gewirth, A. A.; Kenis, P. J. A. Potential Cycling of Silver Cathodes in an Alkaline CO₂ Flow Electrolyzer for Accelerated Stress Testing and Carbonate Inhibition. *ACS Appl. Energy Mater.* **2022**, *5* (10), 12013–12021.
- (59) Kok, J.; de Ruiter, J.; van der Stam, W.; Burdyny, T. Interrogation of Oxidative Pulsed Methods for the Stabilization of Copper Electrodes for CO₂ Electrolysis. *J. Am. Chem. Soc.* **2024**, *146* (28), 19509–19520.
- (60) Sibal, A. P.; Gaines, R. N.; Friel, B. E.; Kenis, P. J. A.; Stillwell, A. S. Turning Waste into Value: Technoeconomic Analysis and Life-Cycle Assessment of Biodiesel-Derived Crude Glycerol Electro-oxidation *Under Review* 2025.
- (61) U.S. Energy Information Administration. U.S. Biodiesel Plant Production Capacity 2022. <https://www.eia.gov/biofuels/biodiesel/capacity/>. (accessed August 16, 2024).
- (62) Bhargava, S. S.; Proietto, F.; Azmoodeh, D.; Cofell, E. R.; Henckel, D. A.; Verma, S.; Brooks, C. J.; Gewirth, A. A.; Kenis, P. J. A. System Design Rules for Intensifying the Electrochemical Reduction of CO₂ to CO on Ag Nanoparticles. *ChemElectroChem* **2020**, *7* (9), 2001–2011.
- (63) Whipple, D. T.; Finke, E. C.; Kenis, P. J. A. Microfluidic Reactor for the Electrochemical Reduction of Carbon Dioxide: The Effect of pH. *Electrochim. Solid-State Lett.* **2010**, *13* (9), No. B109.
- (64) Rachel, N. R.N. GainesResources. <https://rngaines.github.io/main/Gaines-Resources.html>. (accessed June 19, 2025).